ISSN 1063-7745, Crystallography Reports, 2017, Vol. 62, No. 4, pp. 589–596. © Pleiades Publishing, Inc., 2017.
Original Russian Text © G.B. Galiev, E.A. Klimov, S.S. Pushkarev, A.N. Klochkov, I.N. Trunkin, A.L. Vasiliev, P.P. Maltsev, 2017, published in Kristallografiya, 2017, Vol. 62, No. 4, pp. 604–612.

REAL STRUCTURE OF CRYSTALS

Low-Temperature Epitaxial Growth of InGaAs Films on InP(100) and InP(411)*A* Substrates

G. B. Galiev[a,*], E. A. Klimov[a], S. S. Pushkarev[a,*], A. N. Klochkov[a], I. N. Trunkin[b], A. L. Vasiliev[b,], and P. P. Maltsev[a]**

[a] *Institute of Ultra High Frequency Semiconductor Electronics, Russian Academy of Sciences, Moscow, 117105 Russia*
[b] *National Research Centre "Kurchatov Institute," Moscow, 123182 Russia*
**e-mail: serp456207@gmail.com*
***e-mail: a.vasiliev56@gmail.com*

Received September 6, 2016

Abstract—The structural and electrical characteristics of $In_{0.53}Ga_{0.47}As$ epitaxial films, grown in the low-temperature mode on InP substrates with (100) and (411)*A* crystallographic orientations at flow ratios of As_4 molecules and In and Ga atoms of $\gamma = 29$ and 90, have been comprehensively studied. The use of InP(411)*A* substrates is shown to increase the probability of forming two-dimensional defects (twins, stacking faults, dislocations, and grain boundaries), thus reducing the mobility of free electrons, and As_{Ga} point defects, which act as donors and increase the free-electron concentration. An increase in γ from 29 to 90 leads to transformation of single-crystal InGaAs films grown on (100) and (411)*A* substrates into polycrystalline ones.

DOI: 10.1134/S1063774517030063

INTRODUCTION

Semiconductor films of $A^{III}B^{V}$ arsenides (e.g., GaAs, InGaAs, or InAlAs), grown by the molecular-beam epitaxy (MBE) at a low substrate temperature (150–300°C), have been widely investigated due to the peculiar set of their electronic and optical properties. After thermal annealing, low-temperature semiconductor films exhibit high resistivity, high breakdown voltages, and short lifetime of nonequilibrium carriers with a relatively high electron mobility [1–3]. These materials are considered promising for photoconductive antennas: broadband generators and GHz and THz detectors operating in both pulsed and CW modes [4–6]. The investigation of narrow-gap low-temperature InGaAs films on InP substrates is related to the demand for 1.56-μm IR fiber lasers: excitation sources for photoconductive antennas [7].

The specific properties of low-temperature films of $A^{III}B^{V}$ arsenides are due to the nonstoichiometric growth, which causes capture of excess amount of As (up to 2%) during epitaxy [8]. Arsenic is mainly incorporated into the lattice in the form of As_{Ga} antisite defects (As atom in the site of Ga atom) with concentrations on the order of $\sim 10^{20}$ and $\sim 10^{19}$ cm^{-3} in GaAs and InGaAs, respectively [9]. Point defects are responsible for the majority of electronic properties of low-temperature films of $A^{III}B^{V}$ arsenides. In the charged state, they act as electron traps and nonradiative-recombination centers, thus providing extremely short lifetime of photoexcited electrons (less than 1 ps) [10]. The structural changes caused by the arsenic redistribution may occur in low-temperature films during their growth and after the postgrowth annealing. Extended structures (e.g., arsenic precipitates [11, 12]) and various defects (dislocations, twins and stacking faults, or polycrystalline grain boundaries [13]) can be formed. Extended defects cause additional scattering of electrons and reduce their mobility, which is an unfavorable feature of a photoconductive material for THz antennas. Plastic relaxation of low-temperature films is facilitated by the lattice mismatch of the material (due to the arsenic excess) and substrate. For example, after reaching some critical thickness during the MBE growth, a GaAs film undergoes plastic relaxation. This relaxation violates single crystallinity of GaAs film, which continues to grow in the amorphous [14] or polycrystalline [15, 16] phases. At the same time, low-temperature films of $A^{III}B^{V}$ compounds should have (when possible) single-crystal structure to provide high electron mobility in the bulk of material and smooth surface morphology, a necessary condition for implementing planar technology of device production.

The concept of controlling the properties of MBE-grown low-temperature GaAs and InGaAs films using substrates with (*n*11)*A* orientation was proposed in [17]. Different densities of dangling bonds and reconstruction of the (100) and (111) growth surfaces may lead to different conditions of dissociation of As_4 arse-

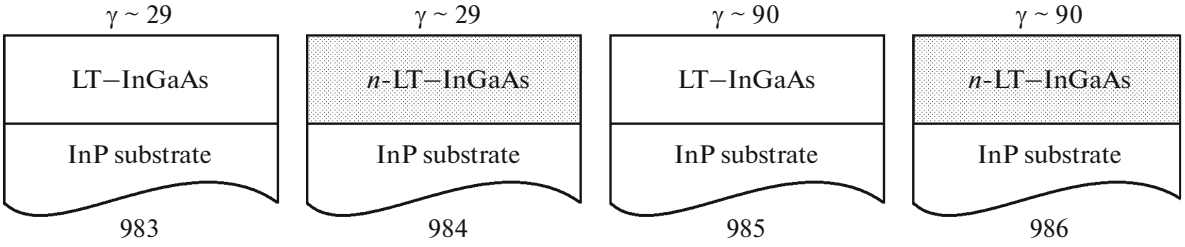

Fig. 1. Design of the samples.

nic molecules on the substrate surface and affect the kinetics of their incorporation into As lattice sites. It is of interest to compare the properties of epitaxial low-temperature InGaAs films, obtained on nonsingular InP substrates and standard InP(100) substrates; however, there are hardly any such data in the literature. In this study, we report the results of analyzing the epitaxial growth of low-temperature InGaAs films on InP(411)*A* substrates with different fluxes of As_4 molecules and their structural and electrical properties in comparison with similar films grown on InP(100) substrates under the same technological conditions.

EXPERIMENTAL

The samples under study were films grown by MBE on semi-insulating Fe-doped InP substrates. The structure of the samples is shown in Fig. 1. They are 1.2-μm-thick low-temperature $In_{0.53}Ga_{0.47}As$ films (LT–InGaAs), grown on surfaces of InP substrates of two types: with (100) and (411)*A* crystallographic orientations. The grown samples were either undoped or homogeneously doped with silicon. The doped samples (984 and 986) were grown at a silicon-cell temperature of 1040°C, which corresponded to the bulk electron concentration of 5×10^{17} cm^{-3} during the high-temperature growth of *n*-GaAs on a GaAs(100) substrate.

Two substrates with (100) and (411)*A* orientations were simultaneously mounted on a sample holder in order to provide identical technological conditions of epitaxial growth of films with the same composition on different substrates. The growth temperature of the LT–InGaAs film was identical for all samples: 200°C. Samples 983 and 984 were grown at a flow ratio of As_4 and III-group elements $\gamma = P_{As4}/(P_{In} + P_{Ga}) \sim 29$, and samples 985 and 986 were grown at $\gamma \sim 90$. After the epitaxial growth the samples were removed from the MBE system and divided in two equal parts. One part was investigated directly after the growth, and the other was studied after annealing in the growth chamber of the MBE system in the As_4 flux at a temperature of 500°C for 1 h. The samples grown on InP(100) and InP(411)*A* substrates were denoted by letters *O* and *A*, respectively.

The sample surface morphology was analyzed by atomic force microscopy (AFM) in a Solver Next microscope (NT MDT). Transverse cuts for the analysis of the sample crystal structure by the standard methods of transmission electron microscopy (TEM) were prepared as follows. After mechanical thinning to 20–40 μm, the samples were additionally thinned by Ar^+ ions in a Gatan 691 system (GATAN, United States) at an accelerating voltage of 5 keV until a hole was formed. The final polishing were performed by Ar^+ ions with an energy reduced to 0.1 keV. The samples were analyzed in a TITAN 80-300 transmission scanning electron microscope (FEI, United States) with a corrector of the probe spherical aberration in the bright- and dark-field modes. The accelerating voltage was 300 kV. The modes of TEM, scanning TEM (STEM), energy-dispersive X-ray microanalysis, and electron diffraction were used for the analysis. The latter mode made it possible to exactly estimate the degree of the film single crystallinity. The electrical parameters of the LT–InGaAs films were determined by measuring the electrical conductivity and Hall coefficient using the van der Pauw method.

SURFACE RELIEF OF SAMPLES

The AFM surface images of the samples under study after thermal annealing are shown in Fig. 2, and the measured values of the root mean square surface roughness (R_q) of the samples before and after annealing are listed in Table 1. It can be seen that the sample surface morphology depends on the orientation of the InP substrate in use and the γ value at which the samples were grown.

For the films grown on the InP(100) substrates at $\gamma \sim 29$, individual pits are observed on a relatively smooth surface (sample 983-*O*). An increases in γ to 90 significantly increases the surface roughness and leads to the formation of a grain relief, in which small grains 0.2–0.3 μm in diameter are grouped into larger agglomerates of irregular shape (0.8–1.6 μm) (sample 985-*O*). The observed regularities in the change in the surface morphology of the LT–InGaAs films on InP(100) substrates in dependence of the As_4 flux (a smoother surface corresponds to a weak As_4 flux and a rougher surface corresponds to an intense As_4 flux) are

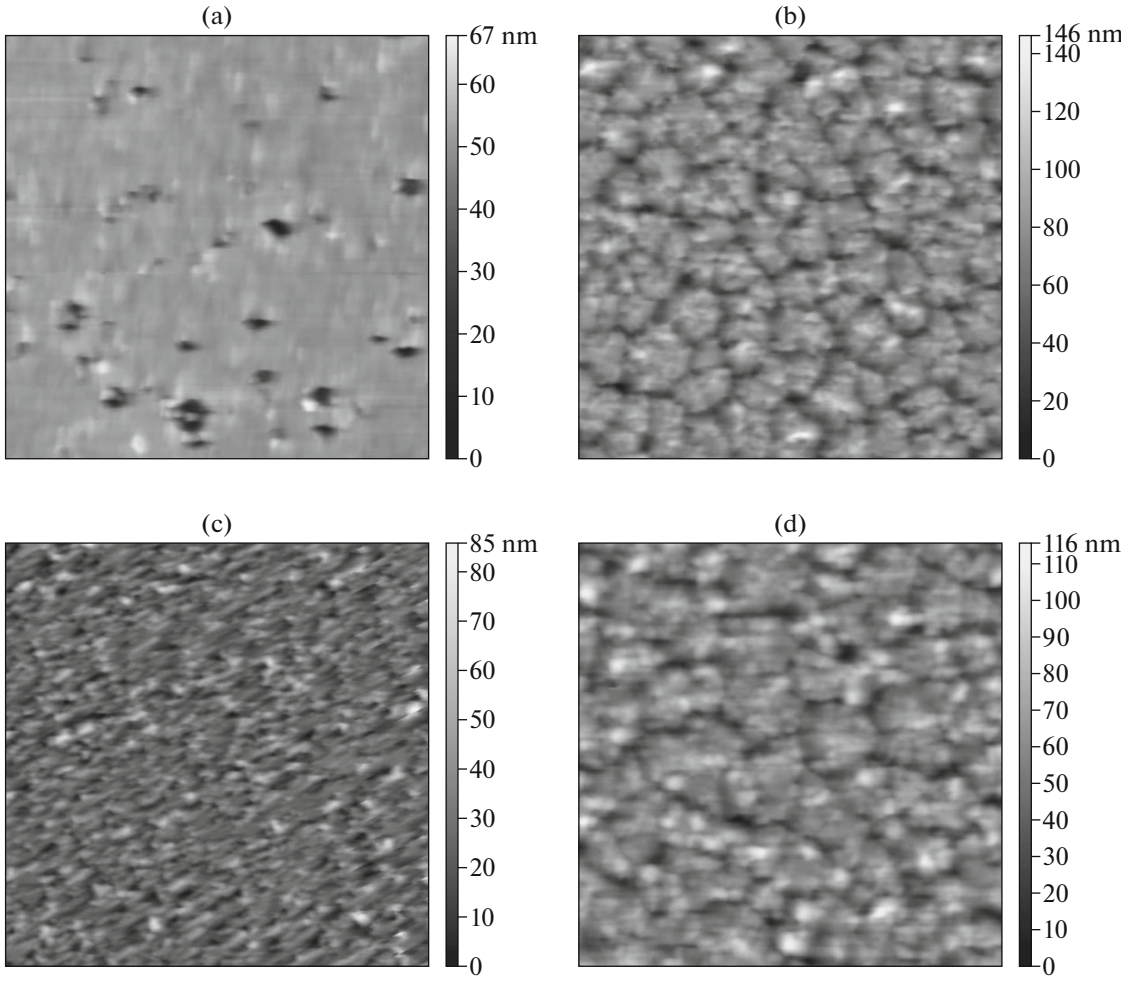

Fig. 2. AFM images (scanning area 10 × 10 μm) of samples (a) 983-*O*, (b) 985-*O*, (c) 983-*A*, and (d) 985-*A* after annealing.

in agreement with the data of [18], obtained for InGaAs films at the same growth temperature (200°C).

The surface of the films grown on the InP(411)*A* substrates at $\gamma \sim 29$ is fine-grained (with grains 0.2–0.3 μm in size). As well as for the samples on the InP(100) substrates, an increase in γ to 90 leads to a large-scale relief with agglomerates 0.8–1.6 μm in size (sample 985-*A*).

It follows from the data of Table 1 that the annealing of the samples obtained on the InP(100) substrates does not affect the surface roughness. At the same time, annealing of the InGaAs films grown on the (411)*A* substrates significantly increases R_q. The surface morphology barely changes after annealing.

SPECIFIC FEATURES OF THE CRYSTALLINE STRUCTURE OF THE SAMPLES

The electron microscopy analysis shows that the sample structure and the features of the extended defects formed therein depend on the substrate orientation and arsenic flow. Let us consider the LT–InGaAs films grown on InP(100) substrates at a relatively low As_4 pressure (P_{As4} = 8 μTorr, γ = 29). Figure 3a shows an electron microscopy image of undoped sample 983-*O*. It is a single crystal consisting of weakly pronounced large domains, which are misoriented with respect to the substrate by an angle of less than 8°. The orientation of all domains is almost identical. It can be seen in Fig. 3 that the domain boundaries may diffuse, as a result of which the domains in the upper part of the film merge, and the film surface becomes relatively smooth. The domain

Table 1. Sample surface roughness

Substrate orientation		(100)		(411)*A*	
Sample		983-*O*	985-*O*	983-*A*	985-*A*
γ		29	90	29	90
R_q, nm	before annealing	3.9	15.9	5.7	7.3
	after annealing	3.7	16.3	9.0	14.3

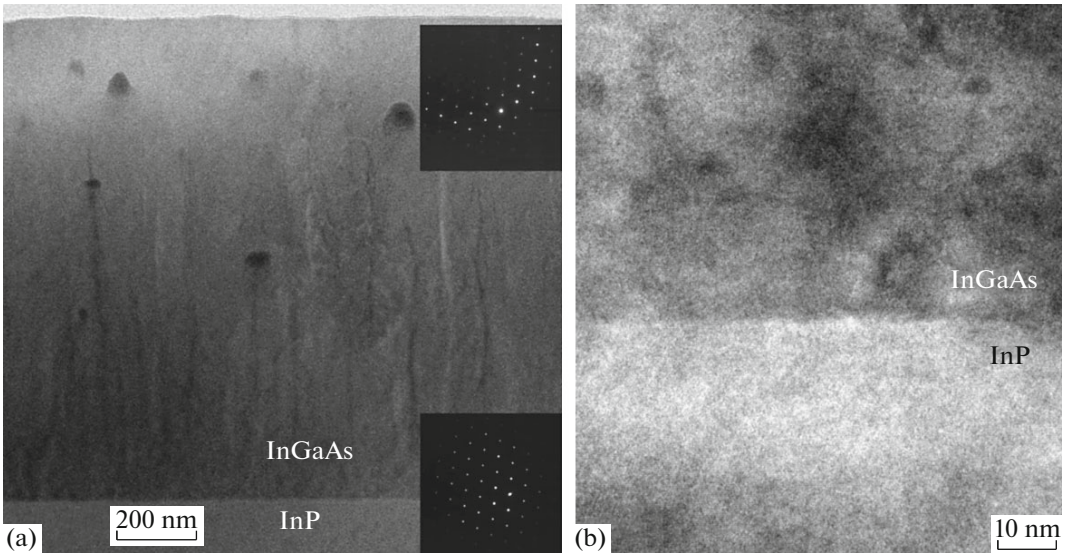

Fig. 3. Bright-field image of the LT–InGaAs film ($\gamma = 29$) grown on an InP(100) substrate (sample 983-*O*) after annealing: (a) full-range photograph and (b) the interface region between the substrate and LT–InGaAs layer. The electron diffraction patterns of the indicated regions are shown in the insets.

single crystallinity is confirmed by the electron diffraction pattern, recorded for the corresponding film region; a deviation of the zone axis, caused by weak domain misorientation, is also observed. The average domain width and height are, respectively, ~90 and ~700 nm. An electron microscopy study of silicon-doped sample 984-*O* shows that it has the same crystal structure as 983-*O;* however, the domains are larger (160 nm wide and 1000 nm high). The domains in the upper film regions are weakly distinguishable. As can be seen in Fig. 3b, the LT–InGaAs film grown on InP(100) has an unbroken crystal structure directly above the substrate (i.e., in the first stage of the MBE process).

Amorphous clusters ~50 nm in size enriched in indium (dark spots in Fig. 3a) were found in sample 983-*O*. An energy-dispersive X-ray microanalysis showed that one of these clusters contained 54% In atoms, 16% Ga atoms, and 30% As atoms, while the neighboring regions of the InGaAs film contained 24% In atoms, 25% Ga atoms, and 51% As atoms. It should be noted that this result was obtained when analyzing not only the cluster but also the regions of the LT–InGaAs film located behind or before the cluster. The cluster is about 50 nm wide; however, its thickness can be smaller because it could be partially cut upon ion thinning of the sample. Thus, the real content of In atoms in the cluster is higher.

Let us consider the LT–InGaAs films grown on InP(411)*A* substrates at $\gamma = 29$. Figure 4a shows an electron microscopy image of undoped sample 983-*O*. One can see that the sample consists of pronounced domains, which are misoriented with respect to each other by an angle of less than several degrees. The domain width and height are, respectively, 80–160 and 160–500 nm. The character of the crystal structure does not change as a result of film bulk doping with Si atoms under the same growth conditions (sample 984-*A*); however, the domains become larger: 180–200 nm wide and ~1000 nm high. As compared to similar films grown on (100) substrates, the concentration of twins and stacking faults and related dislocations in the films formed on InP(411)*A* substrates is higher; however the electron diffraction pattern indicates that domains retain single crystallinity (Fig. 4, inset). Figure 4b presents the interface between the film and the InP(411)*A* substrate; it can be seen that film region with multiple defects is located directly above the substrate. When the LT–InGaAs film thickness reaches ~100–150, this defect region is overgrown, and crystalline domains are formed.

Let us consider the LT–InGaAs film grown at a relatively high pressure of As_4 (P_{As4} = 26 μTorr, γ = 90). Figure 5 shows the electron microscopy images of the LT–InGaAs films grown on substrates with different orientations. Films on InP(100) substrates are mostly polycrystalline. As can be seen in Fig. 5a, only the ~70-nm thick region of the LT–InGaAs film directly over the substrate is single-crystalline. The ~100-nm-thick transition region located above contains single-crystalline regions with unbroken orientation; however, strongly misoriented grains are already present. The grown orientation differs from that of the domains observed in the LT–InGaAs layers obtained at $\gamma = 29$ (grains are arbitrarily oriented with respect to the substrate). In addition, the domain boundaries in the TEM photographs gradually diffuse when approximating the film surface, while the boundaries of the

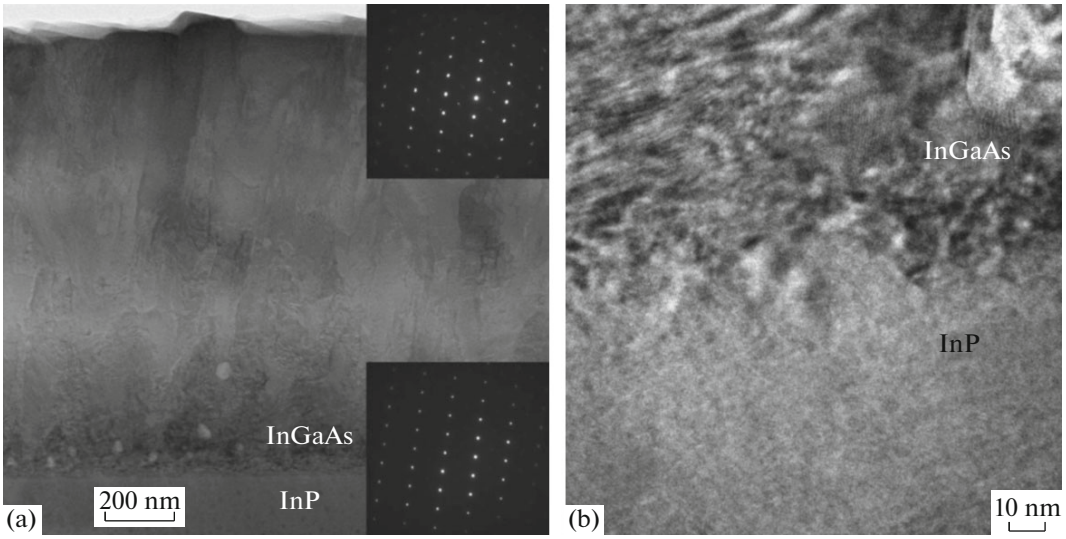

Fig. 4. Bright-field image of the LT–InGaAs film ($\gamma = 29$) grown on an InP(411)*A* substrate (sample 983-*A*) after annealing: (a) full-range photograph and (b) the interface region between the substrate and LT–InGaAs layer. The electron diffraction patterns of the indicated regions are shown in the insets.

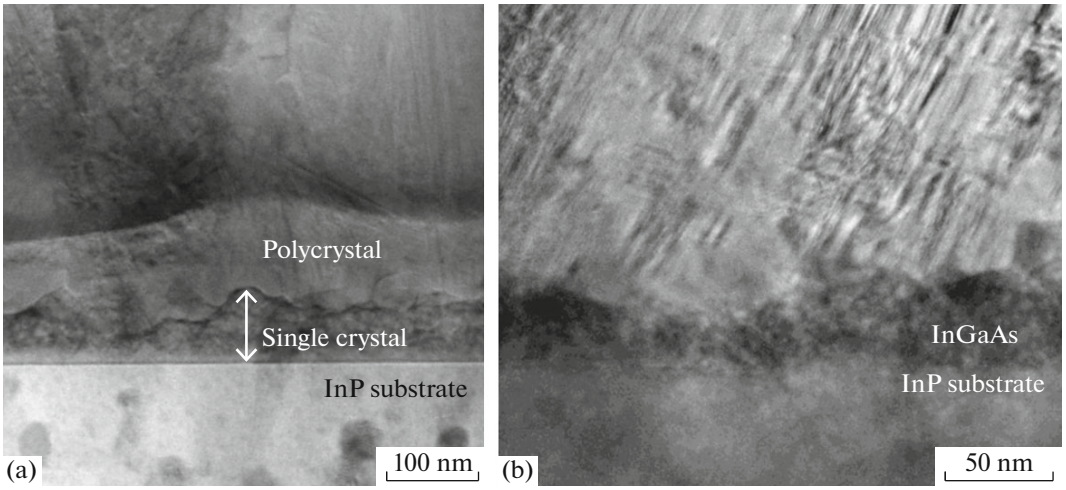

Fig. 5. (a) Bright-field PREM image of sample 985-*O* and (b) bright-field TEM image of sample 986-*A*.

polycrystalline grains remain distinct. The outcrop of grains to the film surface leads to the formation of developed surface morphology with a high roughness, which is due to the misoriented boundaries of grains with different crystallographic orientations.

The grains in the lower part of the film vary in size in the range of 10–70 nm, while the grains in the upper part are 180–200 nm wide and ~600 nm high (sample 985-*O*). As in the case of the LT–InGaAs films grown on InP(100) substrates, domains becomes larger as a result of bulk film doping with Si atoms: they are 150–250 nm wide and ~1000 nm high in doped sample 984-*A*.

The LT–InGaAs films grown on InP(411)*A* substrates at $\gamma = 90$ are completely polycrystalline (samples 985-*A* and 986-*A*). It can be seen in Fig. 5b that a ~50-nm wide transition region is located directly above the substrate, which contains both single-crystal "islands" with retained orientation, less than 10 nm in size, and highly misoriented grains several tens of nanometers in size, after which large elongated grains 160–400 nm wide and ~1000 nm high begin to grow. The polycrystallinity of the samples is confirmed by the electron diffraction patterns recorded for the corresponding film regions. Figure 6 shows an electron diffraction pattern for sample 985-*O*; similar patterns

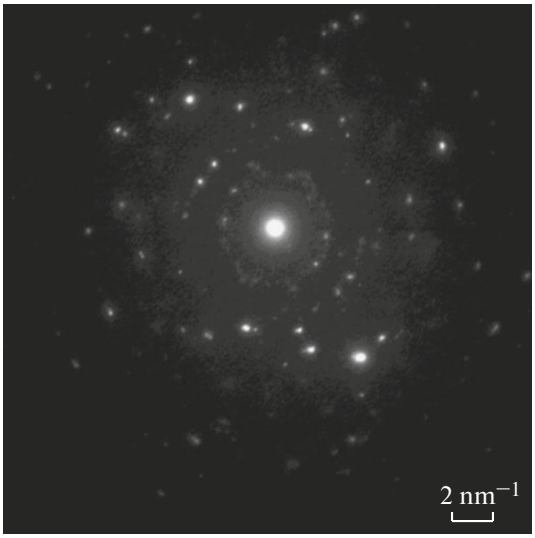

Fig. 6. Electron diffraction pattern of sample 985-*O*.

were obtained for other polycrystalline samples (986-*O*, 985-*A*, and 986-*A*).

ELECTRICAL PARAMETERS

Table 2 contains the measured electrical parameters of the samples. One can see that the free-electron concentration is sufficiently high even for the undoped samples (2.4×10^{17} and 1.0×10^{17} cm^{-3} for samples 983-*O* and 983-*A,* respectively). Although the electron concentration for these samples decreases after annealing, it, nevertheless, remains rather high (~10^{17} cm^{-3}). This value cannot be explained by random doping with background impurities, because the electron concentration in the test satellite samples, grown at typical temperatures of InGaAs growth (400–450°C), was $(2–3) \times 10^{15}$ cm^{-3}. By analogy with a low-temperature GaAs film, the electrical properties of which are explained by the presence of a large number of As_{Ga} antisite defects, forming deep donor levels near the middle of the band gap, one can suggest that the high electron concentration in the LT–InGaAs film is also caused by the high concentration of As_{Ga} defects. The introduction of Si impurity atoms increases the electron concentration in all samples. However, the increase in the electron concentration n_e as a result of doping is much smaller than the dopant concentration.

The electron concentration decreases after annealing for all samples. For identical (but differently doped) samples, the difference in the electron concentration before and after annealing is retained (except for samples 985-*A* and 986-*A*). According to the results of [19], a decrease in n_e indicates a decrease in the concentration of As_{Ga} point antisite defects (which act as electron donors) during annealing. After annealing, the electron mobility significantly increases in all samples due to the decrease in the concentration of defects responsible for electron scattering.

The electron mobility and concentration in the annealed samples grown at $\gamma = 29$ exceed the corresponding values for the similar samples grown at $\gamma = 90$; this circumstance indicates that defects are formed more intensively with an increase in the As_4 flux. The defects include point defects (in particular, As_{Ga} antisite defects), which cause electron scattering and act as electron donors, and one-dimensional and two-dimensional defects (dislocations, twins and stacking faults, and grain boundaries). The presence of polycrystalline grains and the elevated concentration of twins and stacking faults in the samples grown at $\gamma = 90$ were observed by TEM and PREM.

Let us compare the electrical characteristics of the LT–InGaAs films grown on substrates of two types. The electron concentration in the annealed films on InP(411)*A* substrates is $(1–3) \times 10^{16}$ cm^{-3} higher than that in the similar films on InP(100) substrates; this difference may indicate the formation of a larger num-

Table 2. Electrical parameters of the samples (electron mobility μ_e and concentration n_e)

Sample	Substrate orientation	Doping with Si	γ	μ_e, cm^2/(V s)		n_e, 10^{16} cm^{-3}		
				before annealing	after annealing	before annealing	after annealing	Δn_e after annealing
983-*O*	(100)	no	29	800	2500	24	7	–18
983-*A*	(411)*A*	no	29	160	400	10	8	–3
984-*O*	(100)	yes	29	200	950	34	19	–15
984-*A*	(411)*A*	yes	29	350	760	23	21	–2
985-*O*	(100)	no	90	60	340	20	10	–10
985-*A*	(411)*A*	no	90	60	290	21	12	–9
986-*O*	(100)	yes	90	70	320	33	28	–5
986-*A*	(411)*A*	yes	90	70	320	40	31	–9

ber of As_{Ga} antisite defects (playing the role of donors) during film growth on InP(411)*A* substrates. The electron mobility in the films grown on InP(411)*A* substrates at $\gamma = 29$ is lower than that for the similar films on InP(100) substrates, which also indicates some enhancement of the defect formation during the growth of LT–InGaAs films on InP(411)*A* substrates. For the samples grown at $\gamma = 90$, this effect is obscured by a sharply increased number of defects due to the deposition of excess arsenic from the flux.

DISCUSSION

The results of the analysis of the properties of the ~1-μm-thick LT–GaAs films, grown by MBE on GaAs(100) and (111)*A* substrates at a temperature of 230°C and γ ranging from 16 to 45, were reported in [20]. Considering the specific features of their crystal structure, the LT–GaAs and LT–InGaAs films have much in common. It was shown that the LT–GaAs films become polycrystalline after reaching some critical thickness, which decreases with an increase in γ. This critical thickness is also smaller for the growth on a nonsingular GaAs(111)*A* substrate. The twins and stacking faults and small-angle boundaries between domains are conventional defects for both LT–GaAs and LT–InGaAs films [21].

The difference between the LT–InGaAs films analyzed by us and the previously investigated LT–GaAs films is as follows. As precipitates with an internal single-crystal structure and a lattice parameter of ~7 Å were observed in the single-crystal region of the LT–GaAs films by TEM, which is indicated by the presence of moiré in the precipitate images. At the same time, precipitates were not found in the LT–InGaAs films (In-rich amorphous clusters without internal single-crystal structure were found in only one sample). The annealing temperature of 500°C was likely insufficient for the precipitate formation. This is in agreement with the data of [22], where As precipitates were shown to be formed in a low-temperature $In_{0.6}Ga_{0.4}As$ film at an annealing temperature higher than 550°C. According to [9], As precipitates were formed in an LT–$In_{0.53}Ga_{0.47}As$ film after annealing at 600°C.

It follows from the above data that the structure and properties of the LT–InGaAs films grown on InP(411)*A* substrates are similar to a large extent to the structure and properties of the films formed on InP(100) substrates. For example, the values of film surface roughness are close at different orientations of the InP substrates and increase with an increase in the As_4 excess flux. From the structural point of view, the films obtained on substrates of both types at a weak arsenic flow consist of single-crystal domains of similar sizes. Doping films with silicon during MBE leads to an increase in the mean domain size for substrates of both types. This effect is evidently due to the radiative heating of the film growth surface by the hot Si source. Thus, the MBE conditions for the pairs of samples 983/984 and 985/986 are not quite identical with respect to the substrate temperature during growth.

The LT–InGaAs films grown on InP(411)*A* substrates have a number of specific features. For example, the structures of the films near the interfaces with the InP(100) and (411)*A* substrates significantly differ. A single-crystal InGaAs layer with a thickness of about 100 nm is initially grown on the surface of InP with a (100) singular orientation. This layer begins to relax (when the critical thickness is exceeded) due to the accumulation of mechanical stress, and weakly misoriented crystalline domains are formed. The film growth on the InP(411)*A* surface begins with the formation of a polycrystalline region, consisting of crystallites ~10 nm in size with a considerable defect density. This region is gradually overgrown, and larger grains are formed when the film thickness exceeds 100 nm. An increase in the surface roughness after the annealing (which is in agreement with the data of [21]) is also characteristic of the LT–InGaAs films grown on InP(411)*A* substrates. In the case of the (411)*A* orientation, the annealing-induced release of the mechanical stress accumulated during low-temperature growth likely significantly affects the atomic spatial configuration near the film surface.

CONCLUSIONS

The specific features of the crystal structure of the 1.2-μm-thick $In_{0.53}Ga_{0.47}As$ films grown by MBE at a temperature of 200°C on InP substrates were investigated for different As_4 flux pressures and the (100) and (411)*A* crystallographic orientations of the InP substrates.

The AFM analysis of the film surfaces showed that the films grown with a weak As_4 flux ($\gamma = 29$) have a moderately rough surface (R_q = 4–9 nm), while an increase in the As_4 flux ($\gamma = 90$) significantly increases the roughness (R_q = 14–16 nm); in this case, small (0.2–0.3 μm) grains are grouped into larger agglomerates of irregular shape (0.8–1.6 μm). The surface roughness of the films grown on InP(411)*A* nonsingular substrates is somewhat higher.

The TEM and electron diffraction analysis showed that the films grown at $\gamma = 29$ on the (100) and (411)*A* substrates are single crystals consisting of domains; however, the latter are characterized by a high concentration of twins and stacking faults. The films grown at $\gamma = 90$ on (100) substrates are partially polycrystalline (there is a ~70-nm single-crystal region above the substrate), while the films grown on the (411)*A* substrates are completely polycrystalline. The polycrystalline grains are 150–400 nm wide and 600–1000 nm high.

Doping of the LT–InGaAs films with Si atoms increases either the mean size of domains or the mean size of crystalline grains.

The analysis of the electrical parameters of the samples suggested that many As_{Ga} antisite defects are formed on InP(411)*A* substrates during film growth.

Thus, our study showed that the use of InP(411)*A* substrates for epitaxial growth of LT–InGaAs films increases the probability of forming both two-dimensional defects (twin boundaries, stacking faults, dislocations, and grain boundaries), which cause electron scattering and reduce electron mobility, and point defects (As_{Ga} antisite defects), which act as donors and increase the electron concentration. However, the V/III ratio is much more critical for the growth of single-crystal LT–InGaAs, because its increase from 29 to 90 leads to the transformation of the single-crystal films grown on InP(100) and (411)*A* substrates into polycrystalline ones. It should be noted that the optimal conditions for obtaining low-temperature InGaAs layers on InP(411)*A* substrates may be far beyond the range of the growth technological parameters considered above.

ACKNOWLEDGMENTS

We are grateful to O.S. Kolentsova (engineer from the Institute of Functional Nuclear Electronics of the National Research Nuclear University "MEPhI") for carrying out AFM measurements.

This study was supported by the Russian Foundation for Basic Research, project no. 16-29-03294, and the President of the Russian Federation (scholarship SP-686.2016.3).

REFERENCES

1. C. Baker, I. S. Gregory, W. R. Tribe, et al., Appl. Phys. Lett. **85**, 4965 (2004).
2. R. Yano, Y. Hirayama, S. Miyashita, et al., J. Appl. Phys. **94**, 3966 (2003).
3. D. V. Lavrukhin, A. E. Yachmenev, A. S. Bugaev, et al., Semiconductors **49** (7), 911 (2015).
4. A. Krotkus, J. Phys. D: Appl. Phys. **43**, 273001 (2010).
5. I. S. Gregory, C. Baker, W. R. Tribe, et al., IEEE J. Quantum Electron. **41** (5), 717 (2005).
6. G. B. Galiev, E. A. Klimov, D. V. Lavrukhin, et al., Nano Mikrosist. Tekh., No. 6, 28 (2014).
7. A. Takazato, M. Kamakura, T. Matsui, et al., Appl. Phys. Lett. **91**, 011102 (2007).
8. M. Kaminska, Z. Liliental-Weber, E. R. Weber, et al., Appl. Phys. Lett. **54**, 1881 (1989).
9. B. Grandidier, H. Chen, R. M. Feenstra, et al., Appl. Phys. Lett. **74**, 1439 (1999).
10. T. Ouchi and K. Kajiki, U.S. Patent No. 8 835 853 (September 16, 2014) (Canon Kabushiki Kaisha, Tokyo).
11. M. R. Melloch, J. M. Woodall, N. Otsuka, et al., Mater. Sci. Eng. B **22**, 31 (1993).
12. V. V. Chaldyshev, Mater. Sci. Eng. B **88**, 195 (2002).
13. A. Claverie and Z. Liliental-Weber, Mater. Sci. Eng. B **22**, 45 (1993).
14. D. J. Eagleshman, L. N. Pfeiffer, K. W. West, et al., Appl. Phys. Lett. **58** (1), 65 (1991).
15. Z. Liliental-Weber, W. Swider, K. M. Yu, et al., Appl. Phys. Lett. **58** (19), 2153 (1991).
16. J.-F. Roux, J.-L. Coutaz, and A. Krotkus, Appl. Phys. Lett. **74**, 2462 (1999).
17. G. B. Galiev, E. A. Klimov, M. M. Grekhov, et al., Semiconductors **50** (2),195 (2016).
18. M. D. Vilisova, I. V. Ivonin, L. G. Lavrent'eva, et al., Fiz. Tekh. Poluprovodn. **33** (8), 900 (1999).
19. D. C. Look, D. C. Walters, M. O. Manasreh, et al., Phys. Rev. B **42**, 3578 (1990).
20. G. B. Galiev, E. A. Klimov, A. L. Vasil'ev, et al., Crystallogr. Rep. **62** (1), 82 (2017).
21. L. L. Anisimova, A. K. Gutakovskii, I. V. Ivonin, et al., Zh. Strukt. Khim. **45** (7), 96 (2004).
22. J. P. Ibbetson, J. S. Speck, A. C. Gossard, et al., Appl. Phys. Lett. **62**, 2209 (1993).

Translated by Yu. Sin'kov